

## Effect of minor Fe addition on glass forming ability and mechanical properties of $Zr_{55}Al_{10}Ni_5Cu_{30}$ bulk metallic glass

LIU Guang-qiao<sup>1</sup>, KOU Sheng-zhong<sup>1,2</sup>, LI Chun-yan<sup>1</sup>, ZHAO Yan-chun<sup>1</sup>, SUO Hong-li<sup>2</sup>

1. State Key Laboratory of Gansu Advanced Non-ferrous Metal Materials,  
Lanzhou University of Technology, Lanzhou 730050, China;

2. Key Laboratory of Advanced Functional Materials of Ministry of Education,  
Beijing University of Technology, Beijing 100022, China

Received 22 March 2011; accepted 6 November 2011

**Abstract:** A series of rod samples with diameter of 3 mm ( $Zr_{0.55}Al_{0.10}Ni_{0.05}Cu_{0.30}$ )<sub>100-x</sub>Fe<sub>x</sub> ( $x=0, 1, 2, 3, 4$ ) were prepared by magnetic suspend melting and copper mold suction casting method. The effects of a small amount of Fe on glass forming ability (GFA) and mechanical properties of  $Zr_{55}Al_{10}Ni_5Cu_{30}$  bulk metallic glass (BMG) were investigated. The results show that the addition of an appropriate amount (less than 3%, mole fraction) of Fe enhances GFA, as indicated by the increase in the reduced glass transition temperature  $T_{rg}(=T_g/T_l)$  and the parameter  $\gamma(=T_x/(T_g+T_l))$  with increasing Fe content, and GFA gets deteriorated by further Fe addition (4%). The addition of Fe also effectively improves the compressive plasticity and increases the compressive fracture strength in these Zr-based BMGs. Compressive tests on BMG sample with 3 mm in diameter and 6 mm in length reveal work-hardening and a certain plastic strain in the alloy containing 2% Fe. The BMG composite containing 4% Fe also exhibits a high fracture strength along with significant plasticity.

**Key words:** bulk metallic glass; glass forming ability; mechanical properties; microstructure

### 1 Introduction

Since the first report on the synthesis of a bulk metallic glass (BMG) in a special multi-component alloy system by means of copper mold casting in 1989 [1], a number of BMGs have been found in various multi-component alloy systems and attracted much engineering interests [2–4]. The Zr-based BMGs are most expected to be used as engineering materials because they simultaneously have high glass forming ability (GFA), high strength, good toughness, low cost and high corrosion resistance [5–7]. However, as engineering materials, the strength and plasticity of these metallic glasses should be further improved. Especially, the absence of macroscopic plastic strain before fracture at the room temperature limited their applications [8]. Minor addition technique, which has been widely used in other metallurgical fields, is found to be extremely effective in reducing the production cost and is very useful for making good quality BMGs. ECKERT et al [9]

studied the effect of Fe on the glass transition, viscosity of the supercooled liquid and the crystallisation behavior of ( $Zr_{0.65}Al_{0.075}Ni_{0.10}Cu_{0.175}$ )<sub>100-x</sub>Fe<sub>x</sub> and ( $Zr_{0.55}Al_{0.10}Ni_{0.05}Cu_{0.30}$ )<sub>100-x</sub>Fe<sub>x</sub> ( $0 \leq x \leq 15$ ) metallic glasses prepared by rapidly quenched ribbons or mechanically alloying powders. ZHAO et al [10] reported the effect of Fe addition on glass forming ability, hardness, magnetic susceptibility and thermal stability of the Zr–Al–Ni–Cu–Be–Fe metallic glass. However, minor alloying effect of Fe on glass forming ability and mechanical properties of Be-free alloy has not been extensively studied. In view of their physical properties, Fe and Ni are like elements while the former is relatively cheaper. In this work, the known BMG  $Zr_{55}Al_{10}Ni_5Cu_{30}$  is chosen as the starting alloy and Fe as the addition element. The present work is devoted to the preparation and mechanical properties of these Zr–Al–Ni–Cu BMGs.

### 2 Experimental

Multicomponent alloy ingots with nominal

compositions of  $(Zr_{0.55}Al_{0.10}Ni_{0.05}Cu_{0.30})_{100-x}Fe_x$  ( $x=0, 1, 2, 3, 4$ ; mole fraction, %) were prepared from elemental Zr, Cu, Al, Ni and Fe with 99.9% purity in mass fraction by suspend melting under an argon atmosphere using a water-cooled copper crucible. The master alloy was remelted three times in order to obtain chemical homogeneity. Five bulk cylindrical rods with diameter of 3 mm and length of 50 mm were fabricated by copper mold suction casting method, respectively.

The amorphous structure of the sample was identified by X-ray diffraction with Cu  $K_{\alpha}$  radiation (Rigaku D/MAX-2400X diffractometer, diffraction range of  $20^{\circ}$ – $80^{\circ}$ ), and thermal stability associated with glass transition, supercooled liquid region and crystallization was examined by differential scanning calorimetry (DSC) at a constant heating rate of 20 K/min in a flowing argon atmosphere. And the solidus temperature ( $T_s$ ), the liquidus temperature ( $T_l$ ) were examined by differential thermal analysis (DTA) at a constant cooling rate of 20 K/min. The cross-section of as-cast rods and fracture surface were examined by scanning electron microscopy (SEM) on a JEOL JSM-6700 machine, and mechanical properties measurements were performed on a domestic WDW-100D test machine at room temperature under quasi-static loading conditions (strain rate  $8.3 \times 10^{-4} s^{-1}$ ). The samples for compression test were with a size of 3 mm in diameter and 6 mm in length.

### 3 Results and discussion

Figure 1 shows the XRD patterns of as-cast  $(Zr_{0.55}Al_{0.10}Ni_{0.05}Cu_{0.30})_{100-x}Fe_x$  ( $x=0, 1, 2, 3, 4$ ) alloy samples with different contents of Fe.

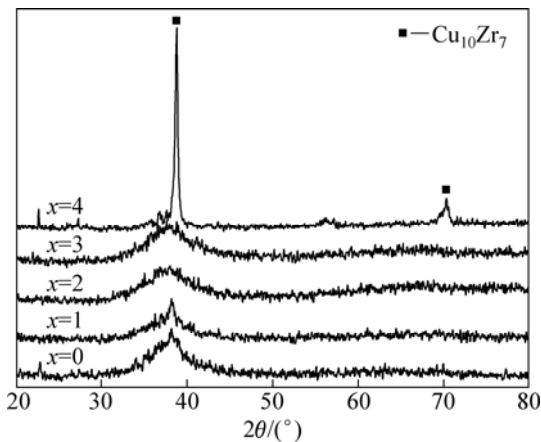


**Fig. 1** XRD patterns of as-cast  $(Zr_{0.55}Al_{0.10}Ni_{0.05}Cu_{0.30})_{100-x}Fe_x$  ( $x=0, 1, 2, 3, 4$ ) samples

A single amorphous phase was achieved in the samples with  $x(Fe)=0, 1, 2$  and  $3$ , as evidenced by a broad diffraction hump in their XRD patterns,

characteristic of glassy materials. Fe and Ni belong to the same transitional subgroup in the elemental periodic table, the atom radius and electronegativity of Fe are close to those of Ni. The GFA of Zr–Cu–Ni–Al–Fe alloy is not significantly changed when less than 3% Fe is added. However, a composite structure of some crystalline phases and amorphous matrix is formed in the sample with  $x(Fe)=4$ , as demonstrated by a few Bragg peaks superimposed on the amorphous diffraction hump. The crystalline phases identified according to the indexing scheme is  $Cu_{10}Zr_7$  phase.

Figure 2 shows DSC and DTA curves of as-cast  $(Zr_{0.55}Al_{0.10}Ni_{0.05}Cu_{0.30})_{100-x}Fe_x$  ( $x=0, 1, 2, 3, 4$ ) alloy samples at a heating rate of 20 K/min.

We can see from Fig. 2(a) that all samples exhibit clear endothermic event associated with the glass transition followed a wide supercooled liquid region, as well as one main exothermic peak, corresponding to the one-step crystallization of amorphous structure, and the obvious melting endothermic peaks. The glass transition temperature  $T_g$ , crystallization onset temperature  $T_x$  are marked by arrows in the DSC curves, and supercooled liquid region  $\Delta T=T_x-T_g$  are listed in Table 1.

It can be seen that, with the increase of Fe content,  $T_g$  increases more rapidly than  $T_x$ , resulting in a decrease

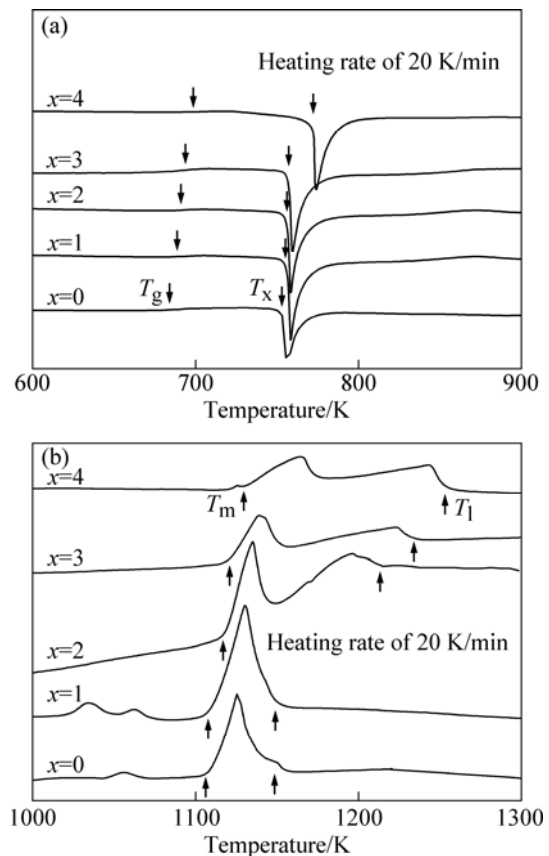


**Fig. 2** DSC (a) and DTA (b) curves of as-cast  $(Zr_{0.55}Al_{0.10}Ni_{0.05}Cu_{0.30})_{100-x}Fe_x$  ( $x=0, 1, 2, 3, 4$ ) samples at heating rate of 20 K/min

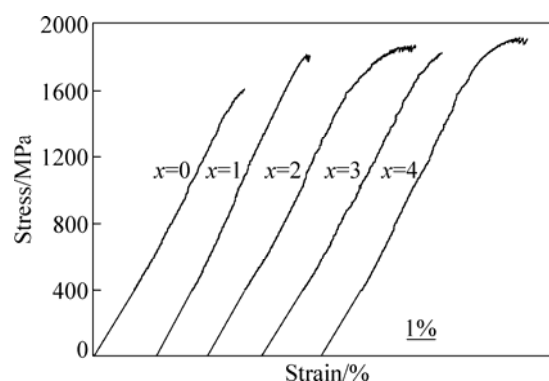
**Table 1** Thermodynamic parameters of as-cast  $(\text{Zr}_{0.55}\text{Al}_{0.10}\text{Ni}_{0.05}\text{Cu}_{0.30})_{100-x}\text{Fe}_x$  ( $x=0, 1, 2, 3, 4$ ) samples

Alloy	$T_g/\text{K}$	$T_x/\text{K}$	$\Delta T_x/\text{K}$	$T_m/\text{K}$	$T_l/\text{K}$	$\Delta T_m/\text{K}$	$T_{rg}$	$\gamma$
$x=0$	672	753	81	1105	1157	52	0.58	0.412
$x=1$	684	761	77	1103	1154	51	0.59	0.414
$x=2$	688	754	66	1115	1211	56	0.57	0.397
$x=3$	691	756	65	1118	1233	95	0.56	0.393
$x=4$	704	767	63	1121	1251	130	0.56	0.392

of  $\Delta T_x$  from 81 K for Fe-free alloy down to 63 K for the alloy containing 4% Fe. To examine the effect of Fe on melting of the Zr-based BMGs, DTA scans up to 1573 K at the same heating rate of 20 K/min were conducted. Figure 2(b) shows the corresponding DTA curves, from which the melting temperature ( $T_m$ ), liquidus temperature ( $T_l$ ) and temperature range for the melting event ( $\Delta T_m=T_l-T_m$ ) can be determined. The resultant data, together with reduced glass transition temperature ( $T_{rg}=T_g/T_l$ ) and parameter ( $\gamma=T_x/(T_g+T_l)$ ), which are usually taken as the gauges for glass forming ability, are also listed in Table 1. One can see that both  $T_m$  and  $T_l$ , exhibit a slightly decrease first at 1% Fe, then an increase with the increase of Fe content for Zr-based alloy samples. Also, as Fe content surpasses 2%, the melting behavior changes from a single peak melting to two, which implies that the addition of an appropriate amount of Fe drives the base system to off-eutectic compositions. In addition, the reduced glass transition temperature  $T_{rg}(=T_g/T_l)$  exhibits a slightly increase first from 0.58 for the Fe-free BMG to 0.59 for the alloy with 1%Fe, then a decrease with the increase of Fe contents to 0.56 for the alloy with 4% Fe. Parameter  $\gamma$  follows the similar trend as  $T_{rg}$ —Fe content variation. The results demonstrate that the addition of appropriate amount of Fe (i.e., 1% in this study) enhances glass forming ability of the basic alloy, which is consistent with the prediction of the “confusion principle” [11]. Fe and Cu have a positive enthalpy of mixing of 13 kJ/mol, the continued addition of Fe (i.e., 2%, 3%, 4% in this study) can induce crystallization and destroy the original amorphous structure, and GFA gets deteriorated.

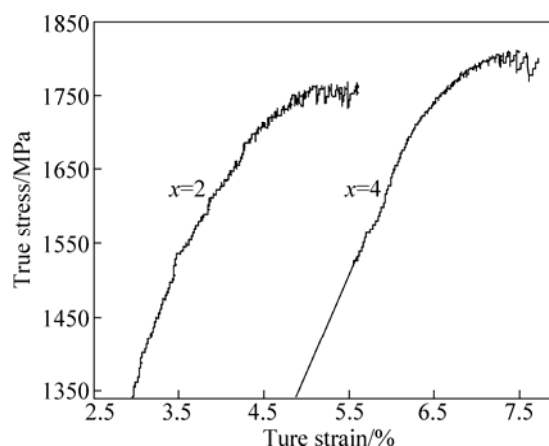
In order to evaluate the mechanical properties of these samples, we carried out quasi-static compression experiments for these alloys. Figure 3 shows the engineering compressive curves of as-cast  $(\text{Zr}_{0.55}\text{Al}_{0.10}\text{Ni}_{0.05}\text{Cu}_{0.30})_{100-x}\text{Fe}_x$  ( $x=0, 1, 2, 3, 4$ ) samples under compressive loading. Their mechanical property data are summarized in Table 2.

It is seen that samples with Fe=1%, 3% underwent a large amount of elastic deformation, followed by a small amount of plastic deformation. Sample with Fe reveals no plastic deformation but a sudden fracture immediately after the elastic limit is reached. The yield strength of sample with  $x(\text{Fe})=4$  ( $R_e=1580$  MPa) is considerably

**Fig. 3** Compressive stress—strain curves of as-cast  $(\text{Zr}_{0.55}\text{Al}_{0.10}\text{Ni}_{0.05}\text{Cu}_{0.30})_{100-x}\text{Fe}_x$  ( $x=0, 1, 2, 3, 4$ ) samples**Table 2** Mechanical properties of as-cast  $(\text{Zr}_{0.55}\text{Al}_{0.10}\text{Ni}_{0.05}\text{Cu}_{0.30})_{100-x}\text{Fe}_x$  ( $x=0, 1, 2, 3, 4$ ) samples

Alloy	Compressive fracture strength, $R_{c,f}/\text{MPa}$	Plastic strain, $A_p/\%$
$x=0$	1614	0
$x=1$	1818	0.15
$x=2$	1868	2.62
$x=3$	1830	0.75
$x=4$	1918	2.19

higher than the value of  $R_e=1385$  MPa obtained for sample with  $x(\text{Fe})=2$ , after yielding, both of them exhibit a strong increase of the stress with further increase in strain, representing a “work-hardening” behavior, which consists of a stage of jerky flow followed by the serrated flow behavior with plastic strain of 2.62%, 2.19% respectively before fracture. Figure 4 shows true stress—true strain curves of  $(\text{Zr}_{0.55}\text{Al}_{0.10}\text{Ni}_{0.05}\text{Cu}_{0.30})_{100-x}\text{Fe}_x$  ( $x=2, 4$ ) alloys obtained from conversion of the engineering stress—strain values. It is very clear that there is an increase in flow stress after yielding. The flow stress values were measured to be from 1340 MPa to 1762 MPa and 1523 MPa to 1810 MPa, respectively, for

**Fig. 4** True stress—true strain curves of as-cast  $(\text{Zr}_{0.55}\text{Al}_{0.10}\text{Ni}_{0.05}\text{Cu}_{0.30})_{100-x}\text{Fe}_x$  ( $x=2, 4$ ) samples

samples with 2%Fe, 4%Fe from true stress—strain diagram.

A serration peak is formed when a dominant shear band overcomes the other intersecting shear bands due to sudden decrease of stress. When this shear band encounters other intersecting shear bands, another serration forms. This process continues till the final fracture takes place [12]. For the shear banding process, there exist two interacting mechanisms [13]: on the one hand, the shear-induced dilation triggers the accumulation of free volume within the shear band, and thus weakens the shear-banding region, leading to the stress drop in the stress—strain curve of metallic glass; on the other hand, a recovery mechanism is also activated by the shear band propagation to counteract the aforementioned softening effect. Therefore, the two counteracting mechanisms lead to the serrated flow as seen in the compressive stress—strain curves for metallic glass. Also, we can see that the compressive fracture strengths of samples with 1%Fe, 2%Fe, 3%Fe, 4%Fe are higher than the sample without Fe, and their compressive fracture strength increments are 204, 254, 216, 304 MPa, respectively. The results demonstrate that the addition of appropriate amount of Fe can increase the compressive fracture strength and improve the compressive plasticity of the basic BMG alloy. There were also reports on the improvement of plasticity by addition of element having positive enthalpy of mixing with other elements [14–17]. For example, addition of Nb to Ni-based [14], Nb and Ag to Cu-based [15,16] and Ta to Zr-based BMGs [17] was reported to enhance the plasticity of the respective alloys. It must be mentioned that excessive addition of Fe (i.e., 4% in this study) leads to the formation of BMG composite, which also can improve the compressive plasticity and increase the compressive fracture strength. This is not consistent with the report [18] that the vulnerable binding zones (between the intermetallic and amorphous matrix) cause alloy brittle and low compressive strength. At present, we cannot explain the phenomenon. So more work and study will be done to elucidate the interesting question.

Figure 5 shows the side views and the fracture morphologies of as-cast  $(\text{Zr}_{0.55}\text{Al}_{0.10}\text{Ni}_{0.05}\text{Cu}_{0.30})_{100-x}\text{Fe}_x$  ( $x=0, 1, 2, 3, 4$ ) alloy samples.

Only a few shear bands can be seen in samples with 1%Fe, 3%Fe (Figs. 5(a), (c)), while a large number of primary and secondary shear bands can be observed for the sample with 2%Fe (Fig. 5(b)), in which most of their width is 2–3  $\mu\text{m}$ , the shear band width (in white circle zones in Fig. 5(b)) are less than 1  $\mu\text{m}$ . It is believed to correspond to the plastic deformation, as evidenced by the serrated peaks in compressive curves in Fig.3. The distribution of shear bands reveals that the propagation of crossed shear bands was hindered and new shear

bands were initiated during the further strain, namely, the multi-stage shear bands were produced during the whole compression test, which results in a large compressive plasticity. The addition elements having positive enthalpy of mixing with constituent elements may provide atom-scale local chemical inhomogeneity or fluctuation in local free volume distribution, affecting the propagation behavior of the shear bands[19]. However, in Fig. 4(d), the shear bands are highly branched, and their movement is rather wavy in nature. This trend suggests that the propagation of shear bands is effectively hindered during the compression process. Hence, the catastrophic shear-off through the whole sample is avoided.

The typical fracture morphology of full bulk amorphous alloys is shown in Figs. 4(a1), (b1), (c1), which is a typical characteristic of fracture feature with well-developed vein patterns. Most of the fracture surface has vein patterns that extend towards the maximum shear stress direction. The local melting signaled by liquid droplet-like morphology can also be observed on the fracture surface of Figs. 4 (a1), (b1), (c1). In Fig. 4(b1), the inset is the enlarged view of the circled zone. In Fig. 4 (d1), although the fracture plane is in an angle of about 45° to the compressive load direction, the fracture surface becomes rough and distorted, and the vein patterns become small, shallow and dim, which may be attributed to complex stress distribution in the sample due to the precipitated crystalline phase. This further leads to the extreme distortion and branching of shear veins as well as evolution of complex intersecting multiple shear bands that avoid the undesired catastrophic failure. This is consistent with the compressive curves in Fig. 3 that the sample with 4% Fe has the highest compressive fracture strength of 1918 MPa and the plastic strain of 2.19%.

## 4 Conclusions

1) The addition of an appropriate amount of Fe (i.e., 1% in this study) can enhance the GFA of  $\text{Zr}_{55}\text{Al}_{10}\text{Ni}_5\text{Cu}_{30}$  base system. Further addition of Fe (i.e., 2%, 3%, 4% in this study) in the base alloy can reduce the GFA as well as the thermal stability.

2) The addition of Fe also can considerably improve the compressive plasticity and increase the compressive fracture strength of  $\text{Zr}_{55}\text{Al}_{10}\text{Ni}_5\text{Cu}_{30}$  base system. The BMG with 2% Fe exhibits the best mechanical properties and reveals work-hardening in the present study.

3) It must be mentioned that excessive addition of Fe (i.e., 4% in this study) leads to the formation of BMG composite, which also can improve the compressive plasticity and increase the compressive fracture strength of  $\text{Zr}_{55}\text{Al}_{10}\text{Ni}_5\text{Cu}_{30}$  base system.

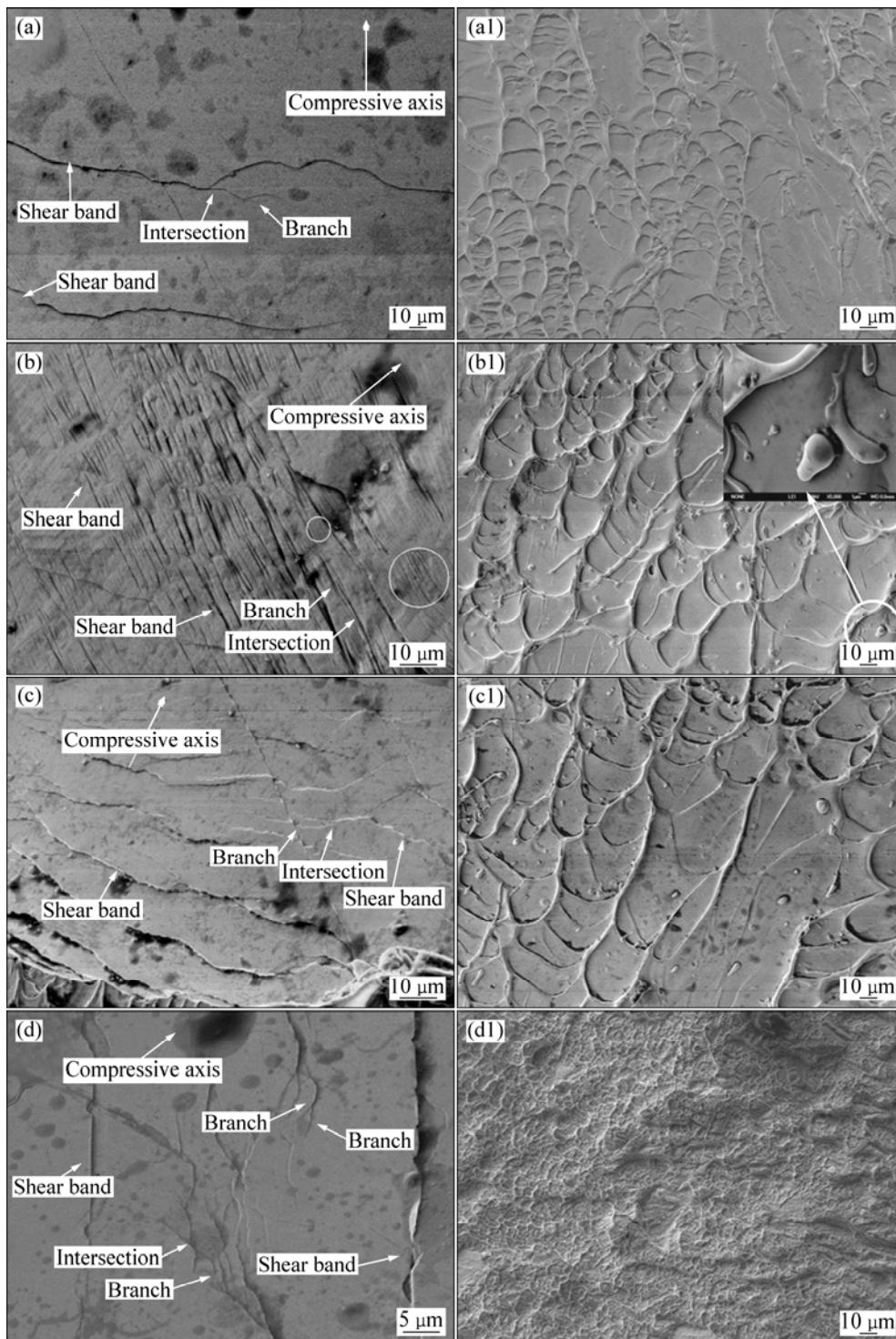


**Fig. 5** Side views of as-cast  $(\text{Zr}_{0.55}\text{Al}_{0.10}\text{Ni}_{0.05}\text{Cu}_{0.30})_{100-x}\text{Fe}_x$  ( $x=0, 1, 2, 3, 4$ ) samples (a, b, c, d) and fracture morphologies (a1, b1, c1, d1): (a, a1)  $x=1$ ; (b, b1)  $x=2$ ; (c, c1)  $x=3$ ; (d, d1)  $x=4$

## References

- [1] INOUE A, ZHANG T, MASUMOTO T. Al–La–Ni amorphous alloys with a wide supercooled liquid region [J]. *Mater Trans*, 1989, 30: 965–972.
- [2] INOUE A, ZHANG W, ZHANG T, KUROSAKA K. High-strength Cu-based bulk glassy alloys in Cu–Zr–Ti and Cu–Hf–Ti ternary systems [J]. *Acta Mater*, 2001, 29: 2645–2652.
- [3] MA H, SHI L L, XU J, LI Y, MA E. Discovering inch-diameter metallic glasses in three-dimensional composition space [J]. *Appl Phys Lett*, 2005, 87: 181915.
- [4] PEKER A, JOHNSON W L. A highly processable metallic glass:  $\text{Zr}_{41.2}\text{Ti}_{13.8}\text{Cu}_{12.5}\text{Ni}_{10.0}\text{Be}_{22.5}$  [J]. *Appl Phys Lett*, 1993, 63: 2342–2344.
- [5] INOUE A, ZHANG T, KIM Y H. Synthesis of high strength bulk amorphous Zr–Al–Ni–Cu–Ag alloys with a nanoscale secondary

- phase [J]. Mater Trans, 1997, 38: 749–755.
- [6] ZHANG Q S, ZHANG W, WANG X M, YOKOYAMA Y, YUBUTA K, INOUE A. Structure, thermal stability and mechanical properties of  $Zr_{65}Al_{17.5}Ni_{10}Cu_{17.5}$  glassy alloy rod with a diameter of 16 mm produced by tilt casting [J]. Mater Trans, 2008, 49: 2141–2146.
- [7] INOUE A, ZHANG T. Fabrication of bulk glassy  $Zr_{55}Al_{10}Ni_5Cu_{30}$  alloy of 30 mm in diameter by a suction casting method [J]. Mater Trans, 1996, 37: 185–187.
- [8] ZHANG Z F, ECKERT J, SCHULTZ L. Difference in compressive and tensile fracture mechanisms of  $Zr_{59}Cu_{20}Al_{10}Ni_8Ti_3$  bulk metallic glass [J]. Acta Mater, 2003, 51: 1167–1179.
- [9] ECKERT J, KÜBLER A, LEONHARD A R, GEBERT A, HEILMAIER M. Glass transition, viscosity of the supercooled liquid and crystallization behaviour of Zr–Al–Cu–Ni–Fe metallic glasses [J]. Mater Trans, 2000, 41: 1415–1422.
- [10] De ZHAO Qian, ZHANG Yong, PAN Ming-xiang, WANG Wei-hua. The effects of iron addition on the glass-forming ability and properties of Zr–Ti–Cu–Ni–Be–Fe bulk metallic glass [J]. Mater Trans, 2000, 41: 1427–1431.
- [11] GREER A L. Materials science-confusion by design [J]. Nature, 1993, 366: 303–304
- [12] TARIQ N H, HASAN B A, AKHTER J I, SHAIKH M A. Evolution of loops in ductile Zr-based bulk metallic glass during plastic deformation [J]. Journal of Alloys and Compounds, 2009, 477: L8–L10.
- [13] YE J C, LU J, YANG Y, LIAW P K. Study of the intrinsic ductile to brittle transition mechanism of metallic glasses [J]. Acta Mater, 2009, 57: 6037–6046.
- [14] LEE M H, LEE J Y, BAE D H, KIM W T, SORDELET D J, KIM D. A development of Ni-based alloys with enhanced plasticity [J]. Intermetallics, 2004, 12: 1133–1137.
- [15] PARK E S, KIM E H, OHKUBO T, HONO K. Enhancement of glass forming ability and plasticity by addition of Nb in Cu–Ti–Zr–Ni–Si bulk metallic glasses [J]. J Non-cryst Sol, 2005, 351: 1232–1238.
- [16] OH J C, OHKUBO T, KIM Y C, FLEURY E, HONO K. Phase separation in  $Cu_{43}Zr_{43}Al_7Ag_7$  bulk metallic glass [J]. Scripta Mater, 2005, 53: 165–169.
- [17] XING L Q, LI Y, RAMESH K T, LI J, HUFNAGEL T C. Enhanced plastic strain in Zr-based bulk amorphous alloys [J]. Phys Rev B, 2001, 64: 180201.
- [18] MAO J, ZHANG H F, FU H M, WANG A M, LI H, HU Z Q. Effects of casting temperature on mechanical properties of Zr-based metallic glasses [J]. Materials Science and Engineering A, 2010, 527: 981–985.
- [19] MONDA K, OHKUBO T, MUKAI T, HONO K. Glass forming ability and mechanical properties of quinary Zr-based bulk metallic glasses [J]. Mater Trans, 2007, 48: 1322–1326.

## 添加微量 Fe 对 $Zr_{55}Al_{10}Ni_5Cu_{30}$ 块体金属玻璃非晶形成能力和力学性能的影响

刘广桥<sup>1</sup>, 寇生中<sup>1,2</sup>, 李春燕<sup>1</sup>, 赵燕春<sup>1</sup>, 索红莉<sup>2</sup>

1. 兰州理工大学 甘肃省有色金属新材料省部共建国家重点实验室, 兰州 730050;

2. 北京工业大学 新型功能材料教育部重点实验室, 北京 100022

**摘要:** 通过磁悬浮熔炼和铜模吸铸法制备直径 3 mm 的  $(Zr_{0.55}Al_{0.10}Ni_{0.05}Cu_{0.30})_{100-x}Fe_x$  ( $x=0, 1, 2, 3, 4$ ) 合金试样, 研究 Fe 元素的微量添加对  $Zr_{55}Al_{10}Ni_5Cu_{30}$  块体金属玻璃非晶形成能力和力学性能的影响。研究表明, 合理添加 Fe 元素(不超过 3%, 摩尔分数)导致约化玻璃转变温度  $T_{rg}(=T_g/T_i)$  和参数  $\gamma(=T_x/(T_g+T_i))$  增大, 因而其非晶形成能力增大, 但添加过量的 Fe 元素(4%)会导致其非晶形成能力的降低。添加 Fe 元素也会显著地改善  $Zr_{55}Al_{10}Ni_5Cu_{30}$  块体金属玻璃的压缩塑性及提高其压缩断裂强度, 当 Fe 元素的添加量为 2% 时, 直径 3 mm、长度 6 mm 的试样在压缩时出现一定的塑性及加工硬化现象。Fe 元素添加量为 4% 形成的金属玻璃基复合材料, 同样也显示良好的压缩塑性和高的压缩断裂强度。

**关键词:** 块体金属玻璃; 非晶形成能力; 力学性能; 组织

(Edited by YANG Hua)